JGR Solid Earth

Key Points:

- Azimuthal anisotropy beneath Central Java is delineated using teleseismic and local S wave splitting with unprecedented spatial resolution
- Most results are consistent with subslab entrained flow traversing a slab window into the mantle wedge and flows parallel to trench
- The vertical component of the escaped flow through the slab window accounts for producing the potassic volcanoes in the back-arc region

Author Contributions:
Funding acquisition: Fansheng Kong, Stephen S. Gao, Kelly H. Liu, Jiabiao Li
Investigation: Fansheng Kong, Stephen S. Gao, Jiabiao Li
Methodology: Kelly H. Liu
Supervision: Stephen S. Gao, Kelly H. Liu, Jiabiao Li
Validation: Fansheng Kong, Stephen S. Gao, Kelly H. Liu
Writing – review & editing: Fansheng Kong, Stephen S. Gao, Kelly H. Liu, Jiabiao Li

Potassic Volcanism Induced by Mantle Upwelling Through a Slab Window: Evidence From Shear Wave Splitting Analyses in Central Java

Fansheng Kong[1,2,3] , Stephen S. Gao[2] , Kelly H. Liu[2] , and Jiabiao Li[1]

[1]Key Laboratory of Submarine Geosciences, Second Institute of Oceanography, Ministry of Natural Resources, Hangzhou, China, [2]Geology and Geophysics Program, Missouri University of Science and Technology, Rolla, MO, USA, [3]Southern Marine Science and Engineering Guangdong Laboratory, Zhuhai, China

Abstract To delineate the mantle flow fields in the vicinity of a previously proposed slab window and the possible roles that they may play in the formation of potassic volcanism in Central Java, we conduct shear wave splitting analyses using both local S and teleseismic XKS waves (including SKS, SKKS, and PKS) recorded by 121 onshore stations and two ocean bottom seismometers (OBSs). The XKS fast orientations from the OBSs are trench normal and in accord with previous subslab anisotropy measurements. In the eastern part of Central Java, the XKS and local S fast orientations from the onshore stations are mostly trench-parallel; in contrast, in the western part of Central Java, the XKS fast orientations are trench-normal while the local S measurements are spatially varying. The observations can be attributed to four flow systems including (a) subslab trench normal mantle flow in areas away from the trench which is entrained by the Australian Plate, (b) trench normal flow that goes into the mantle wedge from the subslab area through a slab window beneath the western part of the study area, (c) trench-parallel subslab flow near the trench beneath the eastern part of the study area which is driven by slab-rollback, and (d) dominantly trench-parallel flow system in the mantle wedge reflecting the horizontal component of the escaped flow system through the slab window. We propose that the vertical component of the escaped flow is responsible for the formation of the potassic volcanoes in the adjacent oceanic area.

Plain Language Summary It has been well established that the vast majority of the world's volcanoes not associated with spreading centers are located along volcanic arcs, ultimately originating from dehydration of water-bearing minerals brought down by subducting oceanic slabs. Some volcanoes occur in areas away from the volcanic arcs and are usually geochemically different from arc volcanoes. The intraplate volcanoes in Central Java are potassic (K)-rich and have been hypothesized to be caused by a supply of volcanic material in the deeper asthenosphere compared to the arc volcanoes. The most frequently cited mechanism is mantle upwelling through a slab window. The window was imaged by some of the seismic tomography studies, but its location is debated due to diminishing resolution at greater depth and limited station coverage. More importantly, whether there is indeed a flow system traversing the slab window remains unrevealed. Here we conducted seismic azimuthal anisotropy investigation using splitting analyses of two kinds of shear waves that are originated at different depths. Our results indicate that mantle flow from the subslab enters the mantle wedge by traversing a slab window, and suggest that the vertical component of this flow system accounts for the formation of the potassic volcanoes in the area.

1. Introduction

Volcanism on Earth is pervasively found at both divergent and convergent plate boundaries, mostly along mid-ocean ridges and above subduction zones. In contrast, volcanic activities away from the plate boundaries, that is, intraplate volcanism, are found in a variety of settings, and their formation mechanisms are debated. In regions adjacent to volcanic arcs, some studies hypothesize that intraplate volcanoes are caused by upwelling mantle flow systems associated with slab breakoffs or slab windows (e.g., Maury et al., 2000; Thorkelson, 1996), although direct evidence for such flow systems is sparse. The chemical compositions of off-arc volcanoes differ from normal arc volcanoes, and the spatial location is independent of the depth of the Wadati-Benioff zone. Examples include volcanoes located in the back-arc region in Central Java (e.g., Hall & Spakman, 2015; Kundu
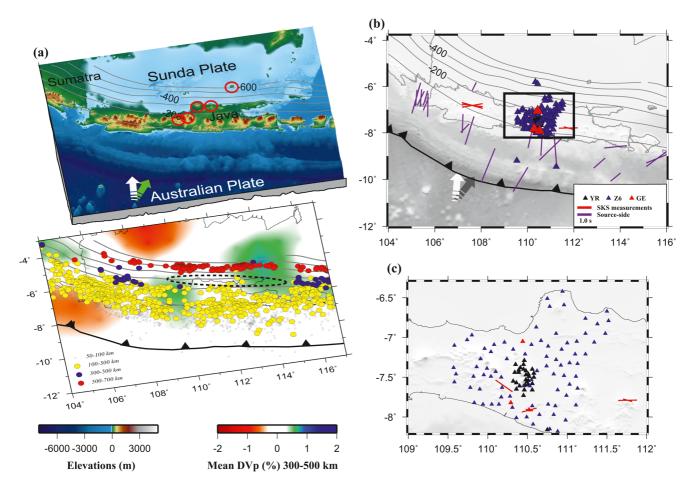
Figure 1. (a) Topographic relief map of the study area with the locations of the potassic volcanoes shown in the red circles (upper plot). The lower plot exhibits the epicenters of earthquakes between 1980 and 2021 with a magnitude larger than 4.0. The background color represents the mean P-wave velocity perturbation between 300 and 500 km depth from Huang et al. (2015). The black dashed ellipse marks the location of the slab window from Hall and Spakman (2015). The green and white arrows stand for the plate motion directions relative to the Sunda Plate (Argus et al., 2011), and in a fixed hotspot reference frame (Gripp & Gordon, 2002), respectively. The contour lines denote the depth of the subducted slab from the Slab2 model (Hayes et al., 2018). (b) A map showing the station locations involved in the study with networks distinguished by different colors, receiver-side shear wave splitting parameters (red bars; Hammond et al., 2010), and the splitting parameters using source-side S waves (purple bars; Lynner & Long, 2014). The length of the bars is proportional to the magnitude of the splitting time and its orientation stands for the fast orientation. (c) A detailed distribution of the broadband seismic stations in the black rectangle of (b).

& Gahalaut, 2011; Setijadji et al., 2006), Mount Etna in Italy (Gvirtzman & Nur, 1999), and the magmatism in the Mediterranean Maghreb margin (Maury et al., 2000).

The back-arc volcanoes in Central Java, for example, Muria and Bawean (Figure 1), are characterized with K-rich magmas (Edwards et al., 1991; Leterrier et al., 1990; Setijadji et al., 2006). Most previous studies propose an asthenospheric origin for the volcanoes, possibly resulted from mantle upwelling associated with a slab window (e.g., Hall & Spakman, 2015; Setijadji et al., 2006). The proposed slab window, which approximately coincides with the location of a seismicity gap in the depth range between 200 and 500 km (Figure 1a), has been suggested by a number of seismic tomographic investigations, but the location, size, and shape of the slab window remain debated (e.g., Amaru, 2007; Huang et al., 2015; Widiyantoro et al., 2011). Additionally, to date, there is a lack of direct geophysical observations on the expected mantle flow system that is assumed to be responsible for the K-rich volcanoes.

The Java trench is currently retreating southward at a rate that increases from the west to the east, from nearly static in western Java to 15 mm/yr in Central Java, and to 21 mm/yr in eastern Java (Schellart et al., 2007). Numerous studies using shear wave splitting (SWS, a tool that the current study employs) have demonstrated that trench retreat and the accompanying slab rollback can induce trench-parallel entrained mantle flow in the subslab

region and trench-normal corner flow in the mantle wedge above the slab (e.g., Becker & Faccenna, 2009; Long & Becker, 2010; Schellart, 2004; Sternai et al., 2014). In addition, driven by the difference of pressure across the subducted slab, part of mantle flow in the subslab may enter the mantle wedge through lateral slab edges or slab windows (e.g., Faccenda & Capitanio, 2013; Fan et al., 2021; Yang et al., 2021). The horizontal component of the various flow systems could be readily characterized and constrained by the strength and orientation of seismic azimuthal anisotropy (Silver & Chan, 1991; Zhang & Karato, 1995). As demonstrated by numerous investigations (e.g., Fouch & Fischer, 1998; Kong et al., 2020; Long & Silver, 2009; Lynner et al., 2017; Silver & Chan, 1991; Yang et al., 2021), splitting of shear waves originated from teleseismic and local events can be used to quantify seismic azimuthal anisotropy and thus delineate the mantle flow fields.

When a sub-vertically propagating shear wave travels through a medium that is azimuthally anisotropic and has an axis of symmetry being horizontal, the shear wave would split into two shear waves that have orthogonal polarization directions and travel in different speed (Ando et al., 1980, 1983; Booth & Crampin, 1985). A splitting delay time (δt), which is associated with the strength and thickness of the anisotropic layer, is accumulated along the raypath as a result of propagating speed differences between the fast and slow waves (e.g., Long & Silver, 2009; Silver & Chan, 1991). The polarization orientation of the fast wave (also termed as fast orientation or ϕ) is closely associated with and can be used to explore the orientation of seismic azimuthal anisotropy (Silver, 1996). The lattice preferred orientation (LPO) of olivine that is the most abundant upper mantle mineral (Ben Ismail & Mainprice, 1998), is generally considered to be responsible for the formation of azimuthal anisotropy in the upper mantle (Zhang & Karato, 1995). A-, C- and E-type olivine fabrics, which are all characterized by a fast orientation of the resulting azimuthal anisotropy that is consistent with the direction of mantle flow, are regarded as the dominant fabric types beneath subducting slabs and in most parts of mantle wedge (Karato et al., 2008).

Previous anisotropy investigations of the Java subduction zone and adjacent regions either use only a limited number of stations (e.g., three stations in Hammond et al., 2010; Figure 1) or focus on anisotropic structures beneath the subducting plate based on splitting measurements of source-side shear waves (e.g., Lynner & Long, 2014; Wang & He, 2020), which mostly suggest a trench orthogonal subslab flow field in the fore-arc region (Figure 1). In this study, teleseismic core-mantle-boundary refracted XKS and local S waves recorded by 123 seismic stations with an unprecedented spatial coverage and resolution are utilized to systematically investigate the anisotropy structure in the mantle wedge and the subslab region in the vicinity of the Java subduction zone, which is aimed at delineating the mantle flow fields above and below the subducted slab, investigating possible modulation of the flow field by the previously proposed slab window, and probing the relationship between the observed anisotropy and the formation of the K-rich volcanoes in the back-arc region of Central Java.

2. Data

In this study, data from a total of 123 broadband seismic stations that resulted in no less than one pair of well-defined local S or teleseismic XKS splitting parameters are used to probe the azimuthally anisotropic structures of the Java subduction zone (Figure 1). The openly accessible seismic data were obtained from three sources, which are elaborated in the Data Availability Statement section. The recording periods of the requested data for the stations varied considerably over the time with a duration of early 1996 to middle 2020 (Figure S1 in Supporting Information S1). The vast majority of the stations were part of two portable seismic experiments, the MERAMEX and DOMERAPI, operated from May 2004 to October 2004 (Wagner et al., 2007) and from October 2013 to April 2015 (Widiyantoro et al., 2018), respectively.

The following two criteria were utilized to request waveform data for the XKS splitting analyses: (a) the epicentral distance between the station and event has a range of 83°–180° for SKS, 95°–180° for SKKS, and 120°–180° for PKS (Figure 2a); (b) the cut-off magnitude is 5.6 for events that have a focal depth less than 100 km, and it is 5.5 for events with greater depth (Liu & Gao, 2013). The events utilized in the analyses of local S splitting have an epicentral distance range from 0° to 7° (Figure 2b) with a cut-off magnitude of 4.0. Wave-type conversions associated with the free surface may cause interference to the local S waves used for SWS analyses. To avoid the influence, only data from events that are within the S-wave window were utilized, which represents a cone-shaped region. The events inside the region have an incidence angle no greater than θ, where θ is calculated by $\sin^{-1} V_S/V_P$ (Booth & Crampin, 1985; Evans, 1984). Using the commonly recognized V_P and V_S velocity ratio of 1.732 (Zandt & Ammon, 1995) leads to a threshold angle of incidence of 35.3°.
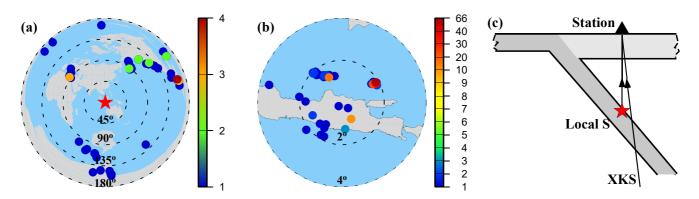
Figure 2. (a) A map of azimuthal equidistant projection illustrating the event distributions which result in no less than one pair of well-defined (Rank A or B) XKS splitting measurements. The color of the solid circles which have a radius of 1° denotes the number of splitting measurements from events in the circles. The dashed circles represent the distance from the center (red star) of Central Java with values labeled in degree. (b) Same as (a) but for events used in the local S splitting analyses. (c) A schematic diagram exhibiting the raypath of two kinds of S waves with different origin depth which are utilized in the study.

3. Methods

For XKS splitting analyses, we utilized the set of approaches described in Liu and Gao (2013) that is based on the method of transverse energy minimization (Silver & Chan, 1991). The optimal splitting measurements correspond to a pair of δt and ϕ that can best minimize the energy on the transverse component after correction. In the process of measuring the splitting parameters using local S waves, the optimal pair of splitting measurements is related to the lesser of the two eigenvalues of the covariance matrix, equivalent to the most-linear particle pattern after correcting the horizontal seismograms based on the optimal pair of splitting parameters (Silver & Chan, 1991). The error estimates of the resulting optimal splitting parameters from both XKS and local S waves are performed by applying the inverse F-test, which stands for the 95% confidence level (Silver & Chan, 1991). In addition, the XKS and local S waveforms were band-pass filtered using corner frequencies of 0.04 and 0.5 Hz, and 0.1 and 1 Hz, respectively, for the purpose of enhancing the signal-to-noise ratio (SNR). The time windows utilized for measuring splitting parameters of the XKS and local S waves were initially set as $(t_a - 5\ \mathrm{s}, t_a + 20\ \mathrm{s})$, and $(t_a - 1\ \mathrm{s}, t_a + 5\ \mathrm{s})$, respectively, where t_a denotes the predicted arrival time of S or XKS measured using the IASP91 Earth model, and were adjusted if needed during the process of manual checking in order to exclude non-XKS or non-local S arrivals.

As detailed in Liu et al. (2008) and Liu and Gao (2013), an objective ranking procedure that is based on the SNR on the radial and transverse components before and after corrections was next applied to all the resulting splitting parameters including the local S and XKS measurements, during which process the measurements were ranked into Quality A (excellent), B (good), C (unusable), and N (null). All the XKS and local S measurements were then manually checked to ensure reliability, and the time window used for measuring the splitting parameters and the rank were adjusted if needed. Examples of splitting measurements measured by using waveforms from the teleseismic XKS and local S events are shown in Figures 3 and 4, respectively. Note that for direct S waves from local events, the radial and transverse directions are not relative to the orientation of the great circle arc but to the initial polarization direction (pre-splitting) of the direct S wave.

4. Results

4.1. Results From XKS Splitting

Totally, 67 pairs of well-defined XKS splitting parameters with a Quality of A or B were obtained at 42 individual seismic stations, including two ocean-bottom-seismometers (OBSs), which are composed of 12 pairs of PKS, 24 pairs of SKKS, and 31 pairs of SKS measurements (Figure 5 and Table S1). The spatial variation of the number of splitting measurements can be found in Figure S2 in Supporting Information S1. In general, the number of well-defined SWS measurements from the OBSs is about two pairs per OBS per year which is comparable to the previous SWS studies utilizing OBS data (e.g., Martin-Short et al., 2015). In comparison, the number for the
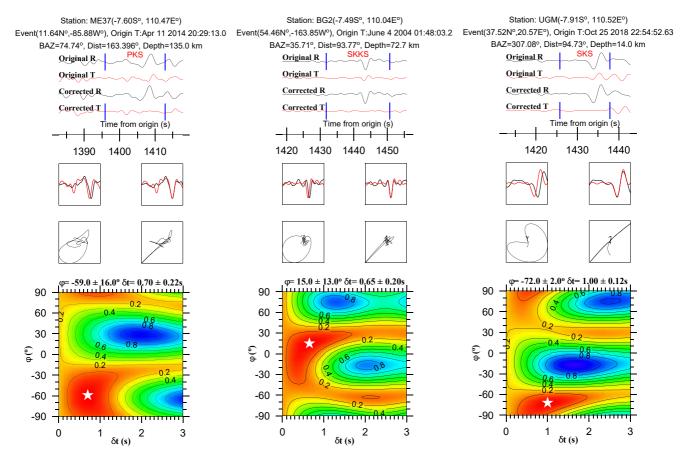
Figure 3. Shear wave splitting examples from PKS, SKKS, and SKS events recorded at Stations ME37 (left column), BG2 (middle), and UGM (right). For each measurement, the plots on the top denote the original and corrected radial (black) and transverse (red) waveforms, the middle plots represent the fast (red) and slow (black) waves before and after moving forward the slow wave by the optimal splitting delay time, patterns of particle motion before (left) and after (right) moving forward the slow wave, and the bottom misfit contour map illustrates the normalized energy computed using waveforms of the corrected transverse component in the time window marked by the two vertical bars in the top panels. The white stars represent the optimal fast orientation and splitting time that result in the minimum misfit.

onshore Z6 stations is about 3 and close to that obtained in the adjacent Sumatra subduction zone per unit time (Kong et al., 2020). Due to (a) the short duration of the majority of the stations (Figure S1 in Supporting Information S1) relative to most other portable seismic experiments and (b) the fact that the area is located less than 83° from areas hosting a significant portion of the XKS events (e.g., Tonga area) for other XKS studies, the number of XKS measurements is not high, although it is comparable to most other XKS studies in terms of the number of measurements per unit area. The splitting times of the XKS splitting measurements have a range of 0.30–2.05 s with a mean value of 1.06 ± 0.05 s. The splitting measurements from the OBSs have a mean of 1.6 ± 0.2 s for δt and a circular average of $34.0 \pm 15.4°$ for ϕ, which is subnormal to the trench strike (about 105° clockwise from the North) and consistent with the relative plate motion direction (RPM) of the Australian Plate relative to the Sunda Plate (36°–39°; Argus et al., 2011) and previous subslab anisotropy measurements (Figure 1b; Lynner & Long, 2014). In contrast, a systematic lateral variation of the XKS fast orientations can be observed at the onshore stations (Figures 5a and 6). For the XKS measurements in the west part of Central Java, the fast orientations are mostly subnormal to the trench strike and consistent with the RPM (red bars shown in Figure S3 of Supporting Information S1). To the east, the ϕ measurements in the arc region are mostly trench-parallel (green bars in Figure S3 of Supporting Information S1) and display a generally clockwise rotational pattern in the back-arc region (Figure 6).

To verify the presence or absence of complex anisotropy associated with multiple-layered (Silver & Savage, 1994) or dipping axis structures (Levin & Park, 1997), a decent back azimuthal coverage of XKS splitting measurements is needed to demonstrate the systematic dependence of ϕ and δt on the back azimuth. The measurements from
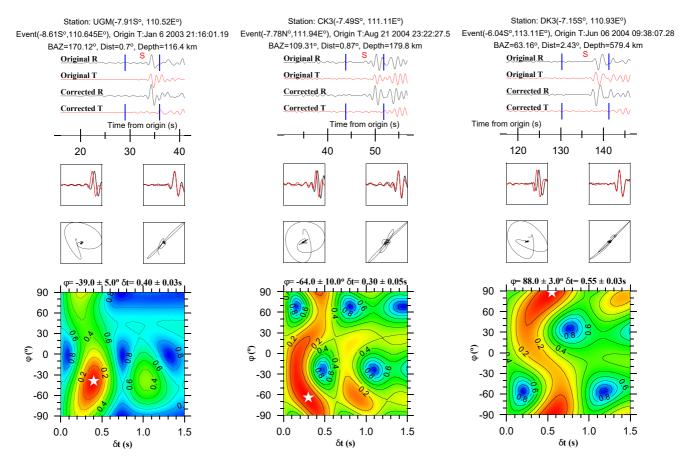
Figure 4. Same as Figure 3 but showing SWS measurements from local S events. The three columns from left to right represent measurements from Stations UGM, CK3, and DK3, respectively.

Station UGM located in the eastern part of Central Java, which cover about two-thirds of the full back azimuth range in the modulo 90° domain, are characterized with insignificant back azimuthal variations (Figure S4 in Supporting Information S1), consistent with the presence of a single layer anisotropy model with a horizontal axis of symmetry (simple anisotropy). For the western part of Central Java, where the stations have a short duration of recording (Figure 1), the (in) dependence of splitting parameters on the back azimuth can be revealed by combining measurements from a number of adjacent stations. As shown in Figure S5 of Supporting Information S1, no systematic azimuthal variations of the splitting parameters are found, suggesting that the measurements can also be adequately attributed to a simple anisotropy model.

4.2. Splitting Results From Local S Events

The local S splitting parameters were obtained at 105 stations (Figure 5b and Table S2). The 197 pairs of Quality A or B measurements were from 43 local earthquakes with focal depths ranging from 22.3 to 594.4 km. For stations located in the arc region, the fast orientations are mostly subparallel to the strike of the Java trench (around 105°) with a circular mean of 127.9 ± 37.4° (Figure 5b) and are approximately normal to the fast orientations of the XKS splitting measurements. The splitting times in this region have a mean of 0.56 ± 0.02 s. In the back-arc region of Central Java, the fast orientations become dominantly oblique to the strike of the trench and are generally in accord with the XKS measurements (Figure 5), with mean values of 76.1 ± 22.5° and 0.54 ± 0.03 s for the fast orientation and splitting time, respectively.
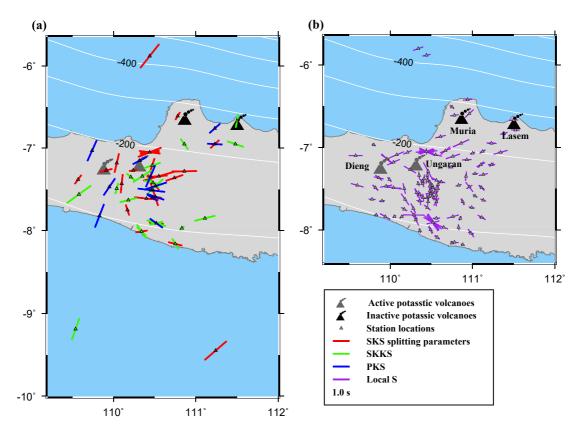
Figure 5. (a) Resulting splitting parameters using XKS phases plotted at station locations. The red, green and blue bars show the SKS, SKKS, and PKS splitting measurements. The triangles represent the locations of the stations. (b) Individual splitting measurements using direct S waves from local events (purple bars) plotted at station locations (triangles). The potassic volcanoes are shown as volcano symbols.

5. Discussion

5.1. Estimation of the Depth of Anisotropy

The densely spaced stations make it feasible to apply the technique that estimates the depth of the layer of anisotropy responsible for the observed XKS splitting parameters based on the spatial coherency (Gao & Liu, 2012). The description of the technique is briefly summarized here. For each candidate anisotropy depth that ranges from 0 to 400 km with a 5 km interval, the coordinates of the XKS ray-piercing points are first computed, and a spatial variation factor, which represents a weighted average of the consistency of the splitting parameters (as measured by the standard deviations of the two splitting parameters) in overlapping rectangle blocks, is computed. The optimal anisotropy depth corresponds to the minimum variation factor. The calculation is conducted with a block size of 0.08°. As shown in Figure 7, the resulting optimal anisotropy depth is 270 km, suggesting that the source of anisotropy accounted for the observed XKS splitting parameters is located in the asthenosphere.

5.2. Mantle Flow From a Slab Window Driven by Slab Rollback

It has been widely established that simple shear originating from the flow gradient generated by the relative movement between the asthenosphere and the overlying lithosphere could produce azimuthal anisotropy with a resulting fast orientation that is consistent with the shear direction (Silver, 1996; Silver & Chan, 1991; Zhang & Karato, 1995). In Central Java, the resulting anisotropy measurements constrained by the local S and teleseismic XKS splitting parameters can be adequately explained by a model invoking mantle flow that enters the mantle wedge from the subslab region through a slab window driven by slab rollback (Becker & Faccenna, 2009; Liu et al., 2019; Long & Becker, 2010; Schellart, 2004). Under this model (Figure 8), the mantle flow from the subslab enters the mantle wedge with a toroidal flow pattern caused by the southward trench retreat and slab rollback, which might be responsible for the abrupt change of XKS fast orientations observed in the arc region of
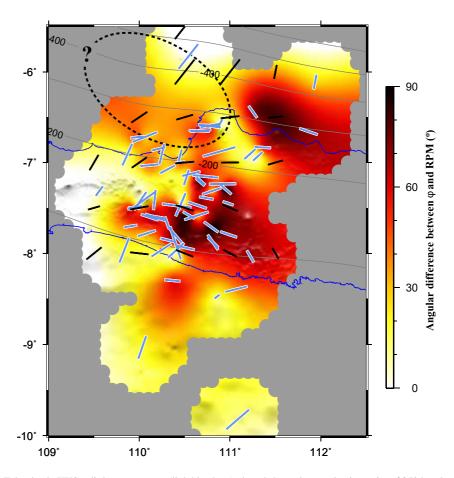
Figure 6. Teleseismic XKS splitting parameters (lightblue bars) plotted above the ray piercing point of 250 km depth. The background color represents the angular difference between the fast orientation measurements and the Australian Plate motion direction relative to the Sunda Plate (Argus et al., 2011). The black bars illustrate the circular mean of the fast orientation and the average of the splitting time for the bins with a radius of 0.5° centered at the bars. The ellipse denotes the favored location of the slab window validated by the local S and XKS splitting measurements with the western edge undefined.

Central Java and the generally clockwise rotational pattern of ϕ observed in the back-arc region (Figure 6). The horizontal component of the flow escaped from the subslab region through the slab window may flow along the trench in the mantle wedge, leading to the fast orientations that are mostly trench-parallel obtained from the local S wave splitting analyses.

Among previous SWS studies in subduction zones, the classical flow model in the mantle wedge involves two-dimensional corner flow associated with the downgoing slab (e.g., Becker & Faccenna, 2009; Fan et al., 2021; Hall et al., 2000) which has a resulting fast orientation generally consistent with subduction direction. This model may explain the western part of the XKS measurements (west of ~110°E) but can not adequately account for the mostly trench-parallel measurements in the eastern part (Figures 5 and 6), and is not consistent with the predicted splitting patterns from numerical and analog modeling studies (e.g., Becker & Faccenna, 2009; Schellart, 2004) when both slab window and slab rollback are present as discussed below.

The slab window is imaged as a hole approximately between 200 and 500 km, but the detailed spatial location is controversial among previous tomography studies (e.g., Amaru, 2007; Huang et al., 2015; Widiyantoro et al., 2011). If we assume that the branch of the subslab flow that goes through the middle of the slab window would largely maintain its original flow direction both before and after passing through the window, the eastern edge of the slab window would be located at the site where ϕ starts to rotate (Figure 8b). Such a mantle flow field is consistent with the slab-rollback-driven flow model suggested by numerical modeling studies (e.g., Becker & Faccenna, 2009) and analog modeling experiments (e.g., Schellart, 2004). Similar abrupt change of ϕ observed
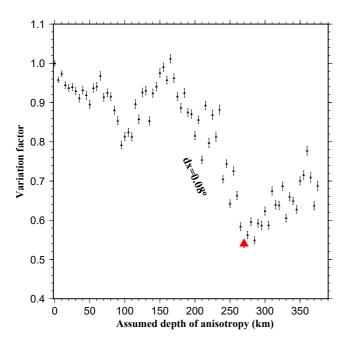
Figure 7. Resulting spatial variation factors plotted with respect to the assumed depth of anisotropy computed by applying the spatial coherency method (Gao & Liu, 2012) using the observed XKS splittings in Central Java. The estimation is conducted with a bin-size (dx) of 0.08°. The optimal depth of anisotropy corresponds to the minimum variation factor and marked with a red triangle on the curve.

in Central Java has also been observed in the western Hellenic (Evangelidis, 2017) and South American subduction zones (Lynner et al., 2017), which have been attributed to slab tears.

5.3. Relationship Between Mantle Flow and Potassic-Rich Volcanoes

One of the simplest models that can explain the resulting splitting measurements using local S and XKS waves involves mantle flow entering the mantle wedge from the subslab region through a slab window, which has been hypothesized to be responsible for the formation of the mantle-driven potassic volcanism in Central Java (e.g., Hall & Spakman, 2015; Kundu & Gahalaut, 2011; Setijadji et al., 2006). As shown in Figure 8, the majority of the potassic volcanoes in the back-arc region of Central Java are located adjacent to the slab window, and along the path of the mantle flow field escaped from the subslab region to the mantle wedge. The only two active K-rich volcanoes, Dieng and Ungaran (Figure 8; Leterrier et al., 1990), are located more closely to the volcanic axis than the others. Such a spatial pattern can be related to the southward migration of the slab window associated with the southward slab rollback. This formation mechanism has been utilized elsewhere to explain the abnormal magmatism for intraplate volcanism, for example, Mount Etna (Gvirtzman & Nur, 1999) and the Afyon alkaline volcanic complex in western Turkey (Prelevic et al., 2015), in which the mantle flow through a slab window either melted lithospheric mantle that was metasomatized during previous subductions with its abnormally high temperature (Maury et al., 2000), or directly provided the enriched source for the distinct chemical composition of intraplate volcanism (e.g., Leterrier et al., 1990; Prelevic et al., 2015; Setijadji et al., 2006).
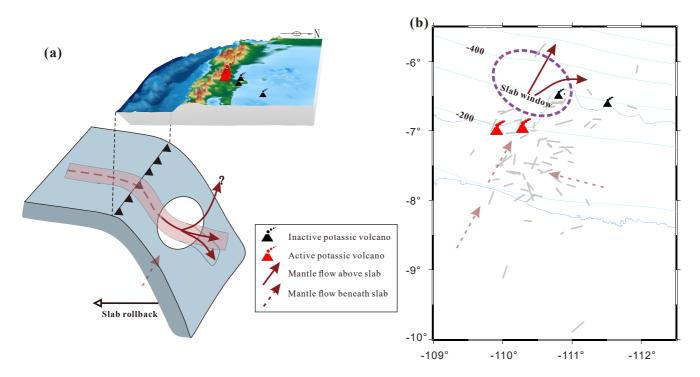

Figure 8. Schematic diagrams showing the mantle flow fields in the upper mantle of the Java subduction zone in a 3D view (a) and a planar view (b). The dashed red arrows denote the mantle flow beneath the subducting slab, while the solid red arrows represent the mantle flow in the mantle wedge above the slab. The gray bars represent the observed XKS splitting parameters. In (a and b) the red and black volcano symbols represent the active (Dieng and Ungaran) and inactive potassic volcanoes, respectively.

6. Conclusions

SWS analyses using both direct S waves from local events and teleseismic XKS phases that were characterized with different origin depth and recorded by both land-based stations and OBSs are used to systematically investigate the azimuthally anisotropic structures in the subslab mantle and the mantle wedge of the Java subduction zone. The two sets of splitting parameters can be explained by a mantle flow system that is driven by the southward slab rollback and enters the mantle wedge through a slab window, causing a trench-parallel subslab mantle flow beneath the arc region and a mostly trench-parallel flow in the mantle wedge. The upwelling component associated with the escaped mantle flow through the slab window may account for the formation of the puzzling back-arc potassic-rich volcanism in Central Java.

Data Availability Statement

All the seismic waveform data used in this study were freely available from three data centers, including (a) the Incorporated Research Institutions for Seismology (IRIS) Data Management Center located in the United States (https://ds.iris.edu/ds/nodes/dmc/data/types/waveform-data; last accessed: April 2020) for Station UGM from Network GE (https://geofon.gfz-potsdam.de/waveform/archive/network.php?ncode=GE), (b) the GEOFON Data Centre of the GFZ German Research Centre for Geosciences (https://geofon.gfz-potsdam.de/waveform/archive; last accessed: April 2020) for Stations SMRI and YOGI from Network GE and 86 stations from Network Z6 (http://www.fdsn.org/networks/detail/Z6_2004), and (c) the RESIF seismic data portal (https://seismology.resif. fr/), a consortium composed of 18 research institutions and universities in France (last accessed: April 2020) under the network code of YR (http://dx.doi.org/10.15778/RESIF.YR2013). The data from IRIS were obtained by using BREQ_FAST (http://ds.iris.edu/ds/nodes/dmc/manuals/breq_fast), while the data from GEOFON and RESIF were requested through the web services using the fdsnws_fetch command (https://www.seiscomp.de/ seiscomp3/doc/applications/fdsnws_fetch.html) and the service interface of timeseries (http://ws.resif.fr/resifws/ timeseries/1/local=en), respectively.

References

Amaru, M. L. (2007). *Global travel time tomography with 3-D reference models* (Ph.D. thesis), Utrecht University.

Ando, M., Ishikawa, Y., & Wada, H. (1980). S-wave anisotropy in the upper mantle under a volcanic area in Japan. *Nature*, *286*, 43–46. https://doi.org/10.1038/286043a0

Ando, M., Ishikawa, Y., & Yamazaki, F. (1983). Shear wave polarization anisotropy in the upper mantle beneath Honshu, Japan. *Journal of Geophysical Research*, *88*, 5850–5864. https://doi.org/10.1029/JB088iB07p05850

Argus, D. F., Gordon, R. G., & DeMets, C. (2011). Geologically current motion of 56 plates relative to the no-net-rotation reference frame. *Geochemistry, Geophysics, Geosystems*, *12*, Q11001. https://doi.org/10.1029/2011GC003751

Becker, T. W., & Faccenna, C. (2009). A review of the role of subduction dynamics for regional and global plate motions. In S. Lallemand, & F. Funiciello (Eds.), *Subduction zone geodynamics* (pp. 3–34). Springer. https://doi.org/10.1007/978-3-540-87974-9_1

Ben Ismail, W., & Mainprice, D. (1998). An olivine fabric database: An overview of upper mantle fabrics and seismic anisotropy. *Tectonophysics*, *296*, 145–157. https://doi.org/10.1016/S0040-1951(98)00141-3

Booth, D. C., & Crampin, S. (1985). Shear-wave polarizations on a curved wavefront at an isotropic free surface. *Geophysical Journal International*, *83*, 31–45. https://doi.org/10.1111/j.1365-246X.1985.tb05154.x

Edwards, C., Menzies, M., & Thirlwall, M. (1991). Evidence from Muriah, Indonesia, for the interplay of supra-subduction zone and intraplate processes in the Genesis of potassic alkaline magmas. *Journal of Petrology*, *32*, 555–592. https://doi.org/10.1093/petrology/32.3.555

Evangelidis, C. P. (2017). Seismic anisotropy in the Hellenic subduction zone: Effects of slab segmentation and subslab mantle flow. *Earth and Planetary Science Letters*, *480*, 97–106. https://doi.org/10.1016/j.epsl.2017.10.003

Evans, R. (1984). Effects of the free surface on shear wavetrains. *Geophysical Journal International*, *76*, 165–172. https://doi.org/10.1111/j.1365-246X.1984.tb05032.x

Faccenda, M., & Capitanio, F. A. (2013). Seismic anisotropy around subduction zones: Insights from three-dimensional modeling of upper mantle deformation and SKS splitting calculations. *Geochemistry, Geophysics, Geosystems*, *14*, 243–262. https://doi.org/10.1002/ggge.20055

Fan, E., He, Y., Ai, Y., Gao, S. S., Liu, K. H., Jiang, M., et al. (2021). Seismic anisotropy and mantle flow constrained by shear wave splitting in central Myanmar. *Journal of Geophysical Research*, *126*, e2021JB022144. https://doi.org/10.1029/2021JB022144

Fouch, M. J., & Fischer, K. M. (1998). Shear wave anisotropy in the Mariana subduction zone. *Geophysical Research Letters*, *25*, 1221–1224. https://doi.org/10.1029/98GL00650

Gao, S. S., & Liu, K. H. (2012). AnisDep: A FORTRAN program for the estimation of the depth of anisotropy using spatial coherency of shear-wave splitting parameters. *Computers & Geosciences*, *49*, 330–333. https://doi.org/10.1016/j.cageo.2012.01.020

Gripp, A. E., & Gordon, R. G. (2002). Young tracks of hotspots and current plate velocities. *Geophysical Journal International*, *150*, 321–361. https://doi.org/10.1046/j.1365-246X.2002.01627.x

Gvirtzman, Z., & Nur, A. (1999). The formation of Mount Etna as the consequence of slab rollback. *Nature*, *401*, 782–785. https://doi.org/10.1038/44555

Hall, C. E., Fischer, K. M., Parmentier, E. M., & Blackman, D. K. (2000). The influence of plate motions on three-dimensional back arc mantle flow and shear wave splitting. *Journal of Geophysical Research*, *105*, 28009–28033. https://doi.org/10.1029/2000JB900297

Hall, R., & Spakman, W. (2015). Mantle structure and tectonic history of SE Asia. *Tectonophysics*, *658*, 14–45. https://doi.org/10.1016/j.tecto.2015.07.003

Hammond, J. O. S., Wookey, J., Kaneshima, S., Inoue, H., Yamashina, T., & Harjadi, P. (2010). Systematic variation in anisotropy beneath the mantle wedge in the Java-Sumatra subduction system from shear-wave splitting. *Physics of the Earth and Planetary Interiors*, *178*, 189–201. https://doi.org/10.1016/j.pepi.2009.10.003

Hayes, G. P., Moore, G. L., Portner, D. E., Hearne, M., Flamme, H., Furtney, M., & Smoczyk, G. M. (2018). Slab2, a comprehensive subduction zone geometry model. *Science*, *362*, 58–61. https://doi.org/10.1126/science.aat4723

Huang, Z., Zhao, D., & Wang, L. (2015). P wave tomography and anisotropy beneath Southeast Asia: Insight into mantle dynamics. *Journal of Geophysical Research*, *120*, 5154–5174. https://doi.org/10.1002/2015JB012098

Karato, S., Jung, H., Katayama, I., & Skemer, P. (2008). Geodynamic significance of seismic anisotropy of the upper mantle: New insights from laboratory studies. *Annual Review of Earth and Planetary Sciences*, *36*, 59–95. https://doi.org/10.1146/annurev.earth.36.031207.124120

Kong, F., Gao, S. S., Liu, K. H., Zhang, J., & Li, J. (2020). Seismic anisotropy and mantle flow in the Sumatra subduction zone constrained by shear wave splitting and receiver function analyses. *Geochemistry, Geophysics, Geosystems*, *21*, e2019GC008766. https://doi.org/10.1029/2019GC008766

Kundu, B., & Gahalaut, V. K. (2011). Slab detachment of subducted Indo-Australian plate beneath Sunda arc, Indonesia. *Journal of Earth System Science*, *120*, 193–204. https://doi.org/10.1007/s12040-011-0056-7

Leterrier, J., Yuwono, Y. S., Soeria-Atmadja, R., & Maury, R. C. (1990). Potassic volcanism in Central Java and South Sulawesi, Indonesia. *Journal of Southeast Asian Earth Sciences*, *4*, 171–187. https://doi.org/10.1016/s0743-9547(05)80011-x

Levin, V., & Park, J. (1997). Crustal anisotropy in the Ural Mountains Foredeep from teleseismic receiver functions. *Geophysical Research Letters*, *24*, 1283–1286. https://doi.org/10.1029/97GL51321

Liu, K. H., & Gao, S. S. (2013). Making reliable shear-wave splitting measurements. *Bulletin of the Seismological Society of America*, *103*, 2680–2693. https://doi.org/10.1785/0120120355

Liu, K. H., Gao, S. S., Gao, Y., & Wu, J. (2008). Shear wave splitting and mantle flow associated with the deflected Pacific slab beneath northeast Asia. *Journal of Geophysical Research*, *113*, B01305. https://doi.org/10.1029/2007JB005178

Liu, L., Gao, S. S., Liu, K. H., Li, S., Tong, S., & Kong, F. (2019). Toroidal mantle flow induced by slab subduction and rollback beneath the Eastern Himalayan syntaxis and adjacent areas. *Geophysical Research Letters*, *46*, 11080–11090. https://doi.org/10.1029/2019GL084961

Long, M. D., & Becker, T. W. (2010). Mantle dynamics and seismic anisotropy. *Earth and Planetary Science Letters*, *297*, 341–354. https://doi.org/10.1016/j.epsl.2010.06.036

Long, M. D., & Silver, P. G. (2009). Mantle flow in subduction systems: The subslab flow field and implications for mantle dynamics. *Journal of Geophysical Research*, *114*, B10312. https://doi.org/10.1029/2008JB006200

Lynner, C., Anderson, M. L., Portner, D. E., Beck, S. L., & Gilbert, H. (2017). Mantle flow through a tear in the Nazca slab inferred from shear wave splitting. *Geophysical Research Letters*, *44*, 6735–6742. https://doi.org/10.1002/2017GL074312

Lynner, C., & Long, M. D. (2014). Sub-slab anisotropy beneath the Sumatra and circum-Pacific subduction zones from source-side shear wave splitting observations. *Geochemistry, Geophysics, Geosystems*, *15*, 2262–2281. https://doi.org/10.1002/2014GC005239

Martin-Short, R., Allen, R. M., Bastow, I. D., Totten, E., & Richards, M. A. (2015). Mantle flow geometry from ridge to trench beneath the Gorda-Juan de Fuca plate system. *Nature Geoscience*, *8*, 965–968. https://doi.org/10.1038/ngeo2569

Maury, R. C., Fourcade, S., Coulon, C., Ei Azzouzi, M., Bellon, H., Coutelle, A., et al. (2000). Post-collisional Neogene magmatism of the Mediterranean Maghreb margin: A consequence of slab breakoff. *Earth and Planetary Sciences*, *331*, 159–173. https://doi.org/10.1016/S1251-8050(00)01406-3

Prelevic, D., Akal, C., Romer, R. L., Mertz-Kraus, R., & Helvacı, C. (2015). Magmatic response to slab tearing: Constraints from the Afyon alkaline volcanic complex, Western Turkey. *Journal of Petrology*, *56*, 527–562. https://doi.org/10.1093/petrology/egv008

Schellart, W. P. (2004). Kinematics of subduction and subduction-induced flow in the upper mantle. *Journal of Geophysical Research*, *109*, B07401. https://doi.org/10.1029/2004JB002970

Schellart, W. P., Freeman, J., Stegman, D. R., Moresi, L., & May, D. (2007). Evolution and diversity of subduction zones controlled by slab width. *Nature*, *446*, 308–311. https://doi.org/10.1038/nature05615

Setijadji, L. D., Kajino, S., Imai, A., & Watanabe, K. (2006). Cenozoic Island arc magmatism in Java Island (Sunda arc, Indonesia): Clues on relationships between geodynamics of volcanic centers and ore mineralization. *Resource Geology*, *56*, 267–292. https://doi.org/10.1111/j.1751-3928.2006.tb00284.x

Silver, P. G. (1996). Seismic anisotropy beneath the continents: Probing the depths of geology. *Annual Review of Earth and Planetary Sciences*, *24*, 385–432. https://doi.org/10.1146/annurev.earth.24.1.385

Silver, P. G., & Chan, W. W. (1991). Shear wave splitting and subcontinental mantle deformation. *Journal of Geophysical Research*, *96*, 16429–16454. https://doi.org/10.1029/91JB00899

Silver, P. G., & Savage, M. K. (1994). The interpretation of shear-wave splitting parameters in the presence of two anisotropic layers. *Geophysical Journal International*, *119*, 949–963. https://doi.org/10.1111/j.1365-246X.1994.tb04027.x

Sternai, P., Jolivet, L., Menant, A., & Gerya, T. (2014). Driving the upper plate surface deformation by slab rollback and mantle flow. *Earth and Planetary Science Letters*, *405*, 110–118. https://doi.org/10.1016/j.epsl.2014.08.023

Thorkelson, D. J. (1996). Subduction of diverging plates and the principles of slab window formation. *Tectonophysics*, *255*, 47–63. https://doi.org/10.1016/0040-1951(95)00106-9

Wagner, D., Koulakov, I., Rabbel, W., Luehr, B.-G., Wittwer, A., Kopp, H., et al. (2007). Joint inversion of active and passive seismic data in Central Java. *Geophysical Journal International*, *170*, 923–932. https://doi.org/10.1111/j.1365-246X.2007.03435.x

Wang, L., & He, X. (2020). Seismic anisotropy in the Java-Banda and Philippine subduction zones and its implications for the mantle flow system beneath the Sunda Plate. *Geochemistry, Geophysics, Geosystems*, *21*, e2019GC008658. https://doi.org/10.1029/2019GC008658

Widiyantoro, S., Pesicek, J. D., & Thurber, C. H. (2011). Subducting slab structure below the eastern Sunda arc inferred from non-linear seismic tomographic imaging. *Geological Society, London, Special Publications*, *355*, 139–155. https://doi.org/10.1144/SP355.7

Widiyantoro, S., Ramdhan, M., Metaxian, J.-P., Cummins, P. R., Martel, C., Erdmann, S., et al. (2018). Seismic imaging and petrology explain highly explosive eruptions of Merapi Volcano, Indonesia. *Scientific Reports*, *8*, 13656. https://doi.org/10.1038/s41598-018-31293-w

Yang, Y., Gao, S. S., Liu, K. H., Kong, F., & Fu, X. (2021). Mantle flow in the vicinity of the eastern edge of the Pacific-Yakutat slab: Constraints from shear wave splitting analyses. *Journal of Geophysical Research*, *126*, e2021JB022354. https://doi.org/10.1029/2021JB022354

Zandt, G., & Ammon, C. J. (1995). Continental-crust composition constrained by measurements of crustal Poisson's ratio. *Nature*, *374*, 152–154. https://doi.org/10.1038/374152a0

Zhang, S., & Karato, S. (1995). Lattice preferred orientation of olivine aggregates deformed in simple shear. *Nature*, *375*, 774–777. https://doi.org/10.1038/375774a0